

Interfacial exchange interactions and magnetism of $\text{Ni}_2\text{MnAl}/\text{Fe}$ bilayers

R. Yanes¹, E. Simon², S. Keller¹, B. Nagyfalusi³, S. Khmelevsky⁴, L. Szunyogh^{2,5} and U. Nowak¹

¹*Department of Physics, University of Konstanz, Germany*

²*Department of Theoretical Physics, Budapest University of*

Technology and Economics, Budafoki út 8., H-111 Budapest, Hungary

³*Institute for Solid State Physics and Optics, Wigner Research Centre for Physics, Hungarian Academy of Sciences, P.O. Box 49, H-1525 Budapest, Hungary*

⁴*Center for Computational Materials Science, Institute for Applied Physics,*

Vienna University of Technology, Wiedner Hauptstrasse 8, A-1060, Vienna, Austria

⁵*MTA-BME Condensed Matter Research Group, Budafoki út 8., H-111 Budapest, Hungary*

Based on a multi-scale calculations, combining *ab-initio* methods with spin dynamics simulations, we perform a detailed study of the magnetic behavior of $\text{Ni}_2\text{MnAl}/\text{Fe}$ bilayers. Our simulations show that such a bilayer exhibits a small exchange bias effect when the Ni_2MnAl Heusler alloy is in a disordered B2 phase. Additionally, we present an effective way to control the magnetic structure of the Ni_2MnAl antiferromagnet, in the pseudo-ordered B2-I as well as the disordered B2 phases, via a spin-flop coupling to the Fe layer.

PACS numbers: 75.50.Ss, 75.60.Jk, 75.70.Cn, 75.30.Gw

I. INTRODUCTION

Antiferromagnets build a class of materials which is used in magnetic multilayer devices, such as GMR sensors or magnetic tunnel junctions, to stabilize and control the magnetization of a ferromagnetic compound. This fact has increased the demand of antiferromagnets and it has led to an increasing interest in novel antiferromagnetic materials, with Heusler alloys as promising candidates for that¹.

Heusler alloys are ternary inter-metallic compounds with the general formula X_2YZ , in which X and Y are typically transition metals and Z is a main group element. This kind of alloys has been in the center of intensive studies in the last decades, mainly due to the wide range of their multifunctional properties. These include magnetic shape memory effects, magneto-caloric and spintronic effects, as well as thermoelectric properties amongst others.²

Heusler alloys can be categorized in two distinct groups by their crystalline structures: half Heusler alloys with the form of XYZ in the C_{1b} structure and full Heusler alloys with the form of X_2YZ in the L_{21} structure³. The unit cell of the L_{21} structure consists of four interpenetrating face-centered cubic (fcc) lattices, while that of the C_{1b} structure is formed by removing one of the X sites. The L_{21} structure transforms into the so-called disordered B2 phase when the Y and Z atoms are mixed, replacing each other at random.

The majority of magnetic Heusler alloys are ferromagnetic though it has been reported that some of them are ferrimagnets or even antiferromagnets. In particular, those compounds with 3d elements where only the Mn atoms carry magnetic moments at Y site are antiferromagnets in the disordered B2 phase. In this context Ni_2MnAl is especially interesting since it has been reported to exhibit an antiferromagnetic behavior in the disordered B2 phase⁴ as well as in the pseudo-order phase

B2-I⁵. The latter is certain limit of the disordered B2 phase, where all the Mn atoms are located in the same (001) plane. Ni_2MnAl in the disordered B2 phase has a perfectly compensated antiferromagnetic ground state, where the Al and Ni atoms possess no net magnetic moment and the site and anti-site Mn atoms are equivalent⁴.

Ni_2MnAl has been in the center of former studies regarding shape memory applications^{6–8} because of its capability to change its magnetic order along with its chemical order. The existence of exchange bias (EB) was reported for Heusler alloys which undergo martensitic phase transitions⁹, for $\text{Ru}_2\text{MnGe}/\text{Fe}$ bilayers¹⁰ and, recently, Tsuchiya et al. published an experimental study of EB in $\text{Ni}_2\text{MnAl}/\text{Fe}$ bilayers¹¹. In general, EB is related to the coupling between a ferromagnet (FM) and an antiferromagnet (AF) and its strength depends on the exchange interaction across the interface and the stability provided by the AF. This calls for a detailed study of the interfacial exchange interactions in $\text{Ni}_2\text{MnAl}/\text{Fe}$ bilayers.

This paper is organized as follows: first we introduce a spin model which is based on first-principles calculations. Then, we analyze the exchange interactions in the bulk and across the interface for the $\text{Ni}_2\text{MnAl}(\text{B2-I}; \text{B2})/\text{Fe}$ interfaces. In the next section, we present spin-dynamics simulations and analyze the possibility to control the magnetic state of the Ni_2MnAl layer via the Fe layer. We finish with a discussion of the origin of a small in-plane EB found in the $\text{Ni}_2\text{MnAl}(\text{B2})/\text{Fe}$ system.

II. MODEL AND NUMERICAL APPROACH

In the following we study the magnetic properties of $\text{Ni}_2\text{MnAl}(\text{B2-I})/\text{Fe}$ and $\text{Ni}_2\text{MnAl}(\text{B2})/\text{Fe}$ interfaces in the spirit of a multi-scale model, linking *ab initio* calculations with dynamical spin model simulations. In terms of the fully relativistic Screened Korringa-Kohn-Rostoker

(SKKR) Green's function method^{12–14} we perform self-consistent calculations of the Ni₂MnAl/Fe bilayers in the disordered local magnetic moment approach¹⁵. We used the general gradient approximation (GGA)¹⁶ in connection with the atomic sphere approximation and an angular momentum cut-off of $l_{max} = 3$. We derive the exchange interactions between the magnetic moments by using the spin-cluster expansion (SCE) technique^{17,18} that provides a systematic parametrization of the adiabatic energy of an itinerant magnetic system. Combining this method with the relativistic disordered local moment (RDLM) scheme^{19,20}, the parameters of the spin-Hamiltonian below can be determined on a quite general level²¹. It is important to note that, due to the relativistic spin-orbit coupling, the exchange interactions between two spins form a 3×3 matrix. Furthermore, since the RDLM-SCE scheme relies on the paramagnetic state as reference, a priori knowledge of the magnetic ground state is not required, which makes it suitable for interface calculations.

The magnetic properties of our system are well described by the following generalized spin model,

$$\mathcal{H} = -\frac{1}{2} \sum_{i,j} \vec{s}_i \mathbf{J}_{ij} \vec{s}_j - \sum_i \vec{s}_i \mathbf{K}_i \vec{s}_i - \sum_i \mu_i \vec{H}_A \vec{s}_i, \quad (1)$$

where the \vec{s}_i represent classical spins, i. e. unit vectors along the direction of each magnetic moment at sites i . The first term stands for the exchange contribution to the energy, with \mathbf{J}_{ij} denoting the tensorial exchange interaction between moment i and j . The second term comprises the on-site anisotropy as well as the magneto-static energy, where \mathbf{K}_i is called the anisotropy matrix. In the presence of an external magnetic field, \vec{H}_A , the last term adds a Zeeman contribution to the Hamiltonian, where μ_i is the magnetic moment of the atom i .

The exchange tensors \mathbf{J}_{ij} can be further decomposed into three parts, $\mathbf{J}_{ij} = J_{ij}^{iso} \mathbf{I} + \mathbf{J}_{ij}^S + \mathbf{J}_{ij}^{A22}$, with the isotropic exchange interaction $J_{ij}^{iso} = \frac{1}{3} \text{Tr}[\mathbf{J}_{ij}]$, the traceless symmetric (anisotropic) part $\mathbf{J}_{ij}^S = \frac{1}{2}(\mathbf{J}_{ij} + \mathbf{J}_{ij}^T) - J_{ij}^{iso} \mathbf{I}$, and the antisymmetric part $\mathbf{J}_{ij}^A = \frac{1}{2}(\mathbf{J}_{ij} - \mathbf{J}_{ij}^T)$. The latter one is clearly related to the Dzyaloshinskii-Moriya (DM) interaction, $\vec{s}_i \mathbf{J}_{ij}^A \vec{s}_j = \vec{D}_{ij} \cdot (\vec{s}_i \times \vec{s}_j)$, with the DM vector \vec{D}_{ij} . The DM interaction arises due to spin-orbit coupling and favors a perpendicular alignment of the spins \vec{s}_i and \vec{s}_j ^{23,24}.

Our first principle calculations show that the Nickel as well as the Alumina atoms have negligible magnetic moments in both phases of the Ni₂MnAl compound, the pseudo-ordered B2-I phase as well as the disordered B2 phase. Therefore we restrict our spin dynamics analysis to the evolution of Fe and Mn moments only.

To study ground state properties along with spin dynamics at zero and finite temperatures we solve the

stochastic Landau-Lifshitz-Gilbert (SLLG) equation,

$$\frac{\partial \vec{s}_i}{\partial t} = -\frac{\gamma}{(1 + \alpha^2)\mu_s} \vec{s}_i \times \vec{H}_i - \frac{\gamma\alpha}{(1 + \alpha^2)\mu_s} \vec{s}_i \times (\vec{s}_i \times \vec{H}_i), \quad (2)$$

by means of Langevin dynamics, using a Heun algorithm^{25,26}. The SLLG equation includes the gyromagnetic ratio γ , a phenomenological damping parameter, α , and the effective field

$$\vec{H}_i = \vec{\zeta}_i(t) - \frac{\partial \mathcal{H}}{\partial \vec{s}_i}, \quad (3)$$

which considers also the influence of a temperature T by adding a stochastic noise term $\vec{\zeta}_i(t)$, obeying the properties of white noise²⁷ with

$$\langle \vec{\zeta}_i(t) \rangle = 0, \quad (4)$$

$$\langle \zeta_i^\eta(t) \zeta_j^\theta(t') \rangle = \frac{2k_B T \alpha \mu_s}{\gamma} \delta_{ij} \delta_{\eta\theta} \delta(t - t'). \quad (5)$$

Here i, j denote lattice sites and η and θ Cartesian components of the stochastic noise.

III. RESULTS AND DISCUSSIONS

A. Ab initio results

For the two cases investigated in this work, the Ni₂MnAl(B2-I)/Fe and Ni₂MnAl(B2)/Fe bilayer, we first calculated the exchange interactions, the magnetic moment and the on-site anisotropy layered resolved with the methods described above. In Fig. 1 the isotropic contribution of the exchange interaction between Mn-Mn and Mn-Fe neighbors are presented as a function of the distance between spin pairs. For the isotropic Mn-Mn exchange interactions our results indicate a similar behavior for the pseudo-ordered B2-I and the disordered B2 phase. The dominant nearest neighbor Mn-Mn exchange interaction, $J_{1,\text{Mn-Mn}} \approx -15$ meV, supports antiferromagnetic order while the magnitude of the exchange interactions between Mn atoms in successive shells decay rapidly (Fig. 1(a)).

The exchange interactions between Mn and Fe atoms across the interface are plotted in Fig. 1(b). The dominant Mn-Fe exchange interaction is again the nearest neighbor one, favoring antiferromagnetic alignment. Remarkably, this interaction is even larger in magnitude than the nearest neighbor Mn-Mn interaction in the bulk. It should also be mentioned that the magnitude of the nearest neighbor exchange interaction in bulk Fe, $J_{1,\text{Fe-Fe}} \approx 50$ meV, is again much larger in magnitude than the above interactions. A summary of the most relevant isotropic exchange parameters is given in Table I.

Another important parameter, which influences the magnetic behavior of a magnetic bilayer and which can

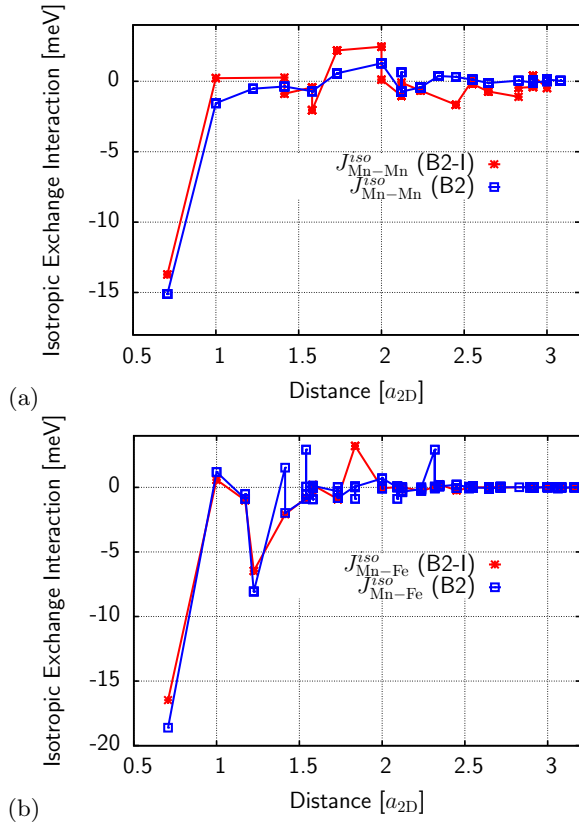


FIG. 1. (Color online). Isotropic exchange interaction as a function of pair distance, (a) between Mn-Mn atoms in B2 and B2-I phases of Ni_2MnAl bulk, (b) across the interface between Mn-Fe atoms in $\text{Ni}_2\text{MnAl}(\text{B2-I})/\text{Fe}$ and $\text{Ni}_2\text{MnAl}(\text{B2})/\text{Fe}$ bilayers.

TABLE I. Calculated maximum isotropic exchange interactions between nearest neighbors, J_{ij}^{iso} (in meV) and magnitudes of the magnetic moment.

Material	$J_{1,\text{Mn-Mn}}^{\text{iso}}$	$J_{1,(\text{Mn-Fe})}^{\text{iso}}$	$J_{1,\text{Fe-Fe}}^{\text{iso}}$	μ_{Mn}	μ_{Fe}
$\text{Ni}_2\text{MnAl}(\text{B2-I})/\text{Fe}$	-13.71	-16.45	52.62	3.32	2.4
$\text{Ni}_2\text{MnAl}(\text{B2})/\text{Fe}$	-15.1	-18.61	52.67	3.35	2.45

lead to the existence of exchange bias is the magnetic anisotropy energy (MAE). It has been reported⁴ that bulk $\text{Ni}_2\text{MnAl}(\text{B2-I})$ has a small in-plane anisotropy with a magnitude of 0.19 meV per spin, while in the case of the perfectly disordered B2 phase the MAE is negligible. Close to the AF/FM interface, however, the magnetic anisotropy is modified. In case of the $\text{Ni}_2\text{MnAl}(\text{B2-I})/\text{Fe}$ interface the preferred magnetic orientation is in-plane with an energy of 0.03 meV in the interface Mn layer and 0.06 meV in the Fe layer. Similarly, an easy plane anisotropy was determined for the $\text{Ni}_2\text{MnAl}(\text{B2})/\text{Fe}$ interface, with a MAE of 0.05 meV and 0.10 meV in the interface Mn and Fe layers, respectively.

B. Spin dynamics simulations

For our spin-dynamics simulations we use the model parameters as determined above from first principles. We suppose the Ni and Al atoms to be nonmagnetic and only consider the dynamics of the Mn and Fe moments. The antiferromagnet is hence modeled by the Mn sub-lattice, forming in total $30 \times 30 \times t_{\text{AF}}$ unit cells and the ferromagnet by $30 \times 30 \times 3$ unit cells, t_{AF} denoting the number of Ni_2MnAl atomic monolayers perpendicular to the interface (in the following labeled $[\text{Ni}_2\text{MnAl}(\text{B2I};\text{B2})]_{t_{\text{AF}}}/[\text{Fe}]_3$). We consider open boundary conditions.

For the case of the disordered B2 phase, the Mn atoms are statistically distributed. The magnitudes of the magnetic moments of Mn and Fe atoms were taken uniformly in the sample using the values given in Table I. Additionally we approximate the effects of the magneto-static interaction in the FM layer as an uniaxial shape anisotropy with $K_{\text{Fe}} = -0.134$ meV and the magnetic hard axis perpendicular to the FM/AFM interface.

In the following sections we will analyze the magnetic properties of the two types of bilayers described above. We evaluate the in-plane hysteresis loops and explore the existence of EB and the switching of the magnetic structure of the Ni_2MnAl layer.

1. Hysteresis in the pseudo-ordered $\text{Ni}_2\text{MnAl}(\text{B2-I})/\text{Fe}$ bilayer

To study the magnetic behavior of this bilayer we calculate hysteresis loops as a succession of quasi-equilibrium states determined by the numerical integration of the SLLG equation applied to the spin model described above. The tensorial exchange interactions are considered up to 11th neighbor. Initially we prepare the system similar to experiments by simulating a field-cooling process. This process starts from a random spin configuration in the AFM at an initial temperature T above the Néel temperature of the AFM but below the Curie temperature of the FM, and proceeds to a final temperature under the influence of an in-plane magnetic H_{FC} .

After the field cooling process Mn as well as Fe magnetic moments are oriented in-plane which is in correspondence with the calculated in-plane magnetic anisotropy. Importantly, the direction of the Mn moments is nearly perpendicular to that of the Fe moments, a consequence of the so-called spin-flop coupling²⁸. Near the interface, the Mn moments are slightly tilted from this perpendicular (x -) direction, leading to a very small net magnetic moment, anti-parallel to the Fe moments. This configuration follows from the strong antiferromagnetic exchange interaction between Mn-Fe moments and the fact that the interface between $\text{Ni}_2\text{MnAl}(\text{B2-I})/\text{Fe}$ is compensated (equal number of Mn moments in both magnetic sub-lattice). This spin configuration is shown

in Fig. 2.

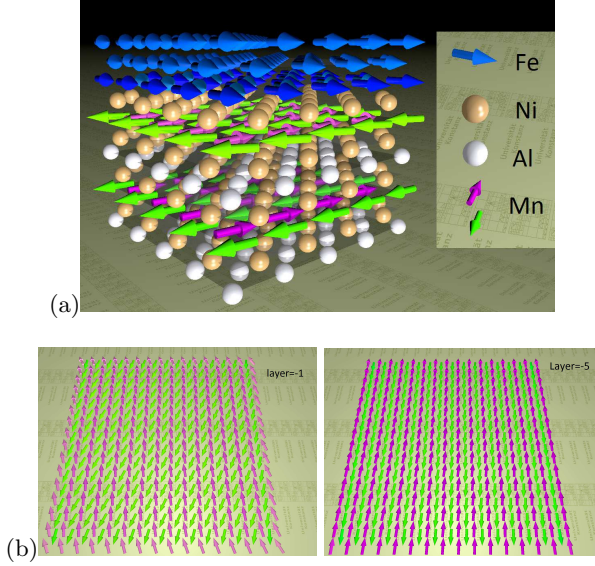


FIG. 2. (Color online). (a) Sketch of the magnetic state of the $\text{Ni}_2\text{MnAl(B2-I)}/\text{Fe}$ interface after the field cooling process. (b) Spin configurations of the first two Mn layers starting at the interface to the Fe (interface Ni layer has layer index 0).

We investigate the switching mechanism and the possible existence of EB for different values of the thickness t_{AF} of the $\text{Ni}_2\text{MnAl(B2-I)}$ layer. Our findings indicate that for perfect bilayers there is no EB within our numerical error of $\pm 75\text{Oe}$. However, the behavior of the AF changes drastically as t_{AF} is increased. As an example in Fig. 3 we show hysteresis loops for two different thicknesses of the AF, focusing on the evolution of the magnetization of the FM along the direction of the applied field, $M_x(\text{FM})$, the total magnetization of the system along the direction of the applied field, $m_h(\text{Tot})$, as well as the in-plane antiferromagnetic order parameter, M_y^{st} , perpendicular to the applied field.

We observe that during hysteresis the Fe moments rotate coherently, staying mostly in-plane. For the smaller thickness, due to the strong exchange interactions between Mn-Fe moments, the small net magnetic moment of the AF close to the interface also rotates, maintaining the antiferromagnetic order. Finally the AF switches following the FM (see Fig. 3 (a)). When the thickness of the AF increases, and concomitantly the relevance of the on-site MAE of the AF, the AF cannot switch anymore and the antiferromagnetic order parameter, M_y^{st} , remains close to unity (see Fig. 3 (b)). Nevertheless, the small canting of the Mn moments at the interface switches with the FM so that the magnetic moment of the AF maintains its direction antiparallel to the Fe moments.

These results indicate that for sufficiently thin layers it is possible to manipulate the magnetic order of the antiferromagnetic Ni_2MnAl layer through the magnetization of the Fe layer. A similar control of the AF magnetization by the FM layer has been reported for

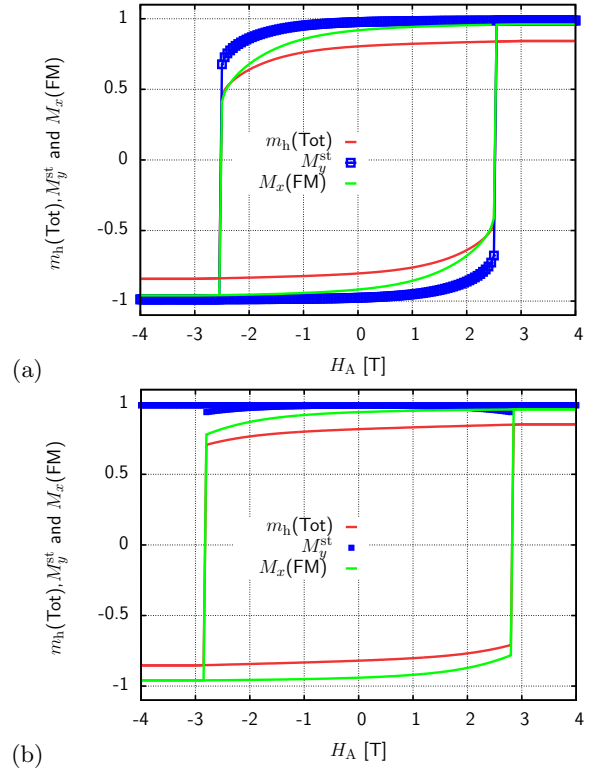


FIG. 3. (Color online). In-plane hysteresis loops for a $[\text{Ni}_2\text{MnAl(B2-I)}]_{t_{\text{AF}}} / [\text{Fe}]_3$ bilayer. (a) thickness of the AF $t_{\text{AF}} = 20a_z$ and (b) $t_{\text{AF}} = 30a_z$. Shown are the normalized magnetization of the FM along the applied field direction, $M_x(\text{FM})$, and the total magnetization of the system along the direction of the applied field, $m_h(\text{Tot})$, as well as the in-plane normalized antiferromagnetic order parameter M_y^{st} perpendicular to the applied field.

$\text{NiFe}/\text{IrMn}/\text{MgO}/\text{Pt}$ heterostructure²⁹ as a key point to the use of that system in an AF-based tunnel junction. Our finding opens hence the door for new Heusler-alloy-based antiferromagnetic spintronic devices.

2. Hysteresis in the disordered $\text{Ni}_2\text{MnAl(B2)}/\text{Fe}$ bilayer

Calculations similar to the ones described above were performed for the disordered $\text{Ni}_2\text{MnAl(B2)}/\text{Fe}$ system. First of all, it is important to note that, as a result of the chemical disorder in the B2 phase and its low effective anisotropy, much more complex spin structures appear in the AF after the field cooling process (see Fig. 4). As before, the Fe moments are aligned along the x -direction, the direction of the field during cooling. Again, we observe a kind of spin-flop coupling with the AF ordered mostly perpendicular to the FM and in-plane. However, the canting of the Mn moments at the interface is much more pronounced as compared to the $\text{Ni}_2\text{MnAl(B2-I)}/\text{Fe}$ system (see the red and yellow Mn moments in the first layer of Fig. 4 b)). The reason for this much stronger canting is the structural disorder in Mn moment posi-

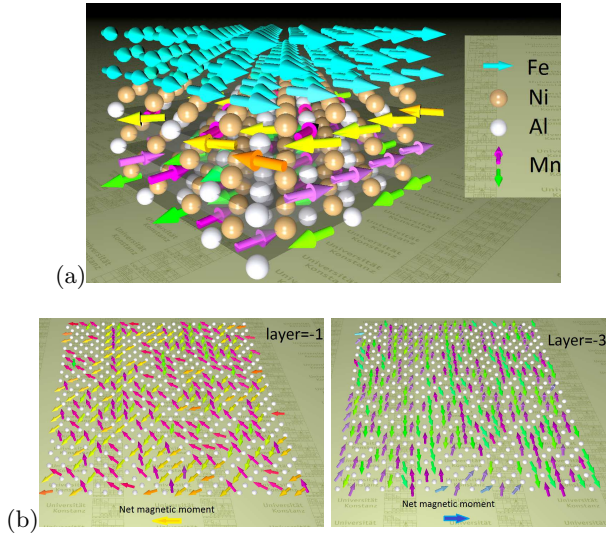


FIG. 4. (Color online). (a) Sketch of the magnetic state of the $[\text{Ni}_2\text{MnAl}(\text{B2})]_{10}/[\text{Fe}]_3$ interface after the field cooling process. (b) Spin configurations of the first two Mn layers starting at the interface to the Fe (interface Ni layer has layer index 0).

tions. Due to the statistical distribution of the Mn moments with some probability clusters of moments within the same sub-lattice appear. In these clusters the moments have a smaller connectivity to Mn moments of the other Mn sub-lattice where the antiferromagnetic exchange would counteract the canting. As a consequence, larger tilting angles and with that a larger net magnetization antiparallel to the Fe magnetization appears. However, the effective coupling between Mn and Fe layers is still smaller since only 50 % of the sites of the layer which is closest to the Fe are occupied. For comparison, in the pseudo-ordered $\text{Ni}_2\text{MnAl}(\text{B2-I})/\text{Fe}$ interface 100% of these sites are occupied by Mn atoms.

In Fig. 5 (a) hysteresis curves are presented. These hysteresis loops are shifted horizontally, corresponding to an exchange bias field of $H_{\text{EB}} = 200 \pm 50 \text{ Oe}$. From the difference between the magnetization of the FM and the total magnetization one can see that not only the Fe moments contribute to the hysteresis loops but also the Mn moments. Furthermore, the sub-lattice magnetization of the AF switches as well indicating that the AF follows the FM as in the case of the pseudo-ordered bilayer for the thin AF layer (see Fig. 5 (c)).

During the switching process the Fe moments rotate again mainly in plane, as we can see in Fig. 5(b) where the x , y and z components of the Fe magnetization are plotted. However a small out-of-plane component of the magnetization appears as well during the switching in both branches of the hysteresis loops. The coercive field is much smaller than in the previous case of the pseudo-ordered bilayer. This smaller coercive field is due to the fact that the effective interface coupling is smaller because of the smaller occupancy with magnetic Mn atoms

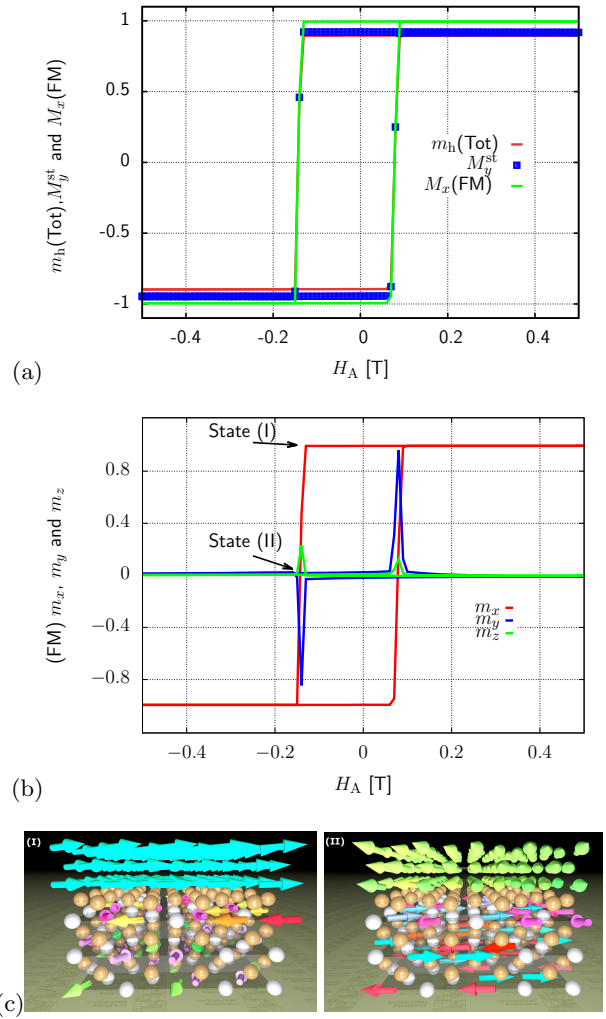


FIG. 5. (Color online). (a) In-plane hysteresis loops for a disordered $[\text{Ni}_2\text{MnAl}(\text{B2})]_{10}/[\text{Fe}]_3$ bilayer. Shown are the normalized magnetization of the FM, $M(\text{FM})$, and the total magnetization of the system along the direction of the applied field, $m_h(\text{Tot})$ as well as the in-plane normalized antiferromagnetic order parameter, $M_{\text{st}}(\text{AF})$, perpendicular to the applied field. (b) Components of the Fe magnetization. (c) Sketches of the magnetic state of the $\text{Ni}_2\text{MnAl}(\text{B2})/\text{Fe}$ bilayer before (I) and during (II) the switching process.

at the interface. Furthermore, the anisotropy of the AF is smaller which leads to a smaller stability of the AF against switching.

For an investigation of the thermal stability of the EB effect mean hysteresis loops were calculated as an average over 5 hysteresis loops performed using the same spatial distribution of Mn-Al atoms. The EB we find is not only rather small and but also unstable against thermal fluctuations (see Fig. 6). Our results suggest a blocking temperature below 100K.

Over all our simulations indicate that the EB is related to the disorder — the lack of perfect compensation due to the random distributions of the Mn and Al atoms into

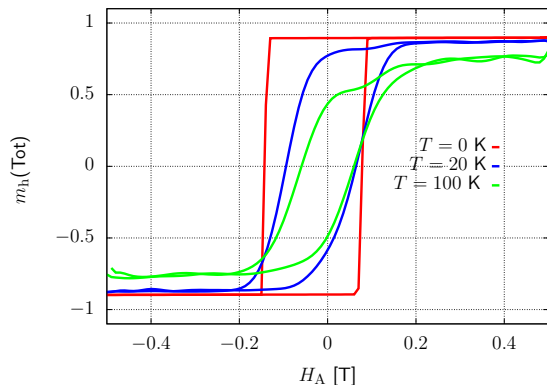


FIG. 6. (Color online). In-plane hysteresis loops for a disordered $[\text{Ni}_2\text{MnAl}(\text{B}2)]_{10}/[\text{Fe}]_3$ bilayer at different temperatures.

the Y-Z positions in the Heusler alloy — in combination with the anisotropy in the AF. As a consequence a small part of the interface magnetization of the AF becomes frozen and does not switch with the FM which leads to the EB. This conclusion is supported by the fact that the EB vanishes for increasing lateral size.

IV. CONCLUSION

In summary, by means of a multi-scale modeling we investigate the interfacial magnetic interactions, the magnetic state and the hysteresis loops of $\text{Ni}_2\text{MnAl}(\text{B}2\text{-I};\text{B}2)/\text{Fe}$ bilayers. Based on first principles calculations we find a strong negative Mn-Fe interface interaction, exceeding the antiferromagnetic interactions within the Ni_2MnAl . For the disordered $\text{Ni}_2\text{MnAl}(\text{B}2)/\text{Fe}$ bilayer we find a small EB at low temperatures in agreement with recent measurements¹¹. The existence of such an exchange bias is related to the disorder in the AF and with that to a lack of perfect compensation at the interface. More importantly, we have shown that it is possible to switch the magnetic structure of the antiferromagnetic Ni_2MnAl layer in both, the pseudo-ordered B2-I and disordered B2 phase, via a spin-flop coupling to the ferromagnetic Fe capping layer. This opens the doors for the control of antiferromagnetic Heusler alloys in spintronic devices with antiferromagnetic components.

ACKNOWLEDGMENTS

This work was supported by the European Commission via the Collaborative Project HARFIR (Project No. 604398) and the National Research, Development and Innovation Office of Hungary under Project No. K115575.

- ¹ A. Hirohata, H. Sukegawa, H. Yanagihara, I. Zutic, T. Seki, S. Mizukami, and R. Swaminathan, *IEEE Trans. Magn.* **51**, 1 (2015)
- ² T. Graf, C. Felser and S.S.P. Parkin, *Prog. Solid Stat. Chem.* **39**, 50 (2011).
- ³ P. J. Webster and K. R. A. Ziebeck, *Heusler Alloys*, in Landolt-Bronstein New Series Group III, Vol. 19C, H. R. J. Wijn (Ed.) (Springer, Berlin, 1988) p. 75.
- ⁴ E. Simon, J. Gy. Vida, S. Khmelevsky and L. Szunyogh, *Phys. Rev. B* **92**, 054438 (2015).
- ⁵ I. Galanakis and E. Şaşıoğlu, *Appl. Phys. Lett.* **98**, 102514 (2011).
- ⁶ M. Acet, E. Duman, E. F. Wassermann, L. Mañosa and A. Planes, *J. Appl. Phys.* **92**, 3867 (2002).
- ⁷ T. Büsgen, J. Feydt, R. Hassdorf, S. Thienhaus, M. Moske, M. Boese, A. Zayak and P. Entel, *Phys. Rev. B* **70**, 014111 (2004).
- ⁸ V. K. Srivastava, S. K. Srivastava, R. Chatterjee, G. Gupta, S. M. Shivprasad and A. K. Nigam, *Appl. Phys. Lett.* **95** 114101 (2009).
- ⁹ A. Behler, N. Teichert, B. Dutta, A. Waske, T. Hickel, A. Auge, A. Httten and J. Eckert, *AIP Advanced* **3**, 122112 (2013).
- ¹⁰ J. Balluff, M. Meinert, J.-M. Schmalhorst, G. Reiss, and E. Arenholz, *J. Appl. Phys.* **118**, 243907 (2016).
- ¹¹ T. Tsuchiya, T. Kubota, T. Sugiyama, T. Huminiuc, A. Hirohata and K. Takanashi, *J. Phys. D: Appl. Phys.* **49**, 235001 (2016).
- ¹² L. Szunyogh, B. Ujfalussy, P. Weinberger, and J. Kollár, *Phys. Rev. B* **49**, 2721 (1994).
- ¹³ R. Zeller, P. H. Dederichs, B. Ujfalussy, L. Szunyogh, and P. Weinberger, *Phys. Rev. B* **52**, 8807 (1995).
- ¹⁴ L. Szunyogh, B. Ujfalussy, and P. Weinberger, *Phys. Rev. B* **51**, 9552 (1995).
- ¹⁵ B. L. Gyorffy, A. J. Pindor, J. B. Staunton, G. M. Stocks, H. Winter, *J. Phys F: Met. Phys.* **15**, 1337 (1985).
- ¹⁶ J.P. Perdew, S. Burke, M. Ernzerhof, *Phys. Rev. Lett.* **77**, 3865 (1996)
- ¹⁷ R. Drautz, and M. Fähnle *Phys. Rev. B* **69**, 104404 (2004).
- ¹⁸ R. Drautz, and M. Fähnle *Phys. Rev. B* **72**, 212405 (2005).
- ¹⁹ J. B. Staunton, S. Ostanin, S. S. A. Razee, B. L. Gyorffy, L. Szunyogh, B. Ginatempo, E. Bruno, *Phys. Rev. Lett.* **93**, (2004)
- ²⁰ J. B. Staunton, L. Szunyogh, A. Buruzs, B. L. Gyorffy, S. Ostanin, L. Udvardi, *Phys. Rev. B* **74**, 144411, (2003).
- ²¹ L. Szunyogh, L. Udvardi, J. Jackson, U. Nowak, and R. Chantrell, *Phys. Rev. B* **83** 024401 (2011).
- ²² L. Udvardi, L. Szunyogh, K. Palotás, and P. Weinberger, *Phys. Rev. B* **68**, 104436 (2003).
- ²³ I. Dzyaloshinskii, *J. Phys. Chem. Solids* **4**, 241 (1958).
- ²⁴ T. Moriya, *Phys. Rev.* **120**, 91 (1960).
- ²⁵ J. L. García-Palacios and F. J. Lázaro, *Phys. Rev. B* **58**, 14937 (1998).
- ²⁶ U. Nowak, in *Handbook of Magnetism and Advanced Magnetic Materials*, Micromagnetism Vol. 2, edited by H. Kronmüller and S. Parkin, (Wiley, Chichester, 2007).

- ²⁷ A. Lyberatos, D. Berkov, and R. Chantrell, *Journal of Physics: Condensed Matter* **5**, 8911 (1993).
- ²⁸ N. C. Koon, *Phys. Rev. Lett.* **78**, 4865 (1998).
- ²⁹ B. G. Park, J. Wunderlich, X. Martí, V. Holý, Y. Kurosaki, M. Yamada, H. Yamamoto, A. Nashide, J. Hayakawa, H. Takahashi, A. B. Shick and T. Jungwirth, *Nat. Materials* **10**, 347 (2011).